Sudan University for Sciences and Technology

College of Graduate Studies

Estimation of Radiation Dose during Chest Computed Tomography Examinations

تقدير الجرعة الأشعاعية أثناء فحوصات الصدر بالاشعة المقطعية المحوسبة

A thesis Submitted for Partial Fulfillment for the Requirement of MSc Degree in Diagnostic Radiological Imaging

By:

Abdulrahman Salahudeen Abdullateef Mohammed

Supervisor:

Dr. Ahmed Mostafa Abukonna

February 2018

قال تعالى:

(وَيَسْأَلُونَكَ عَنِ الرُّوحِ ۖ قُلِ الرُّوحُ مِنْ أَمْرِ رَبِّي وَمَا أُوتِيتُم مِّنَ الْعِلْمِ إِلَّا قَلِيلًا)

الاسراء(85)

Dedication

To my beloved kind mother

To my Great father

To all knowledge seekers

I dedicate this work

Acknowledgment

"I humbly thank Allah Almighty, the Merciful and the Beneficent, who gave me health, thoughts and cooperative people to enable me achieve this goal."

Special vote of thanks to my supervisor:

Dr. /Ahmed Mustafa Abu konna.

My thanks to everyone who helps me in way or another to make this work appear to light.

List of Figures

List of Tables

List of Abbreviations

Abbreviation	Full meaning
AEC	Automatic Exposure Control
CT	Computed tomography
CTDI	Computed Tomography Dose Index
DLP	Dose Length Product
DRLs	Diagnostic Reference Levels
ED	Effective Dose
HRCT	High Resolution Computed Tomography
IAEA	International Atomic Energy Agency
ICRP	International Commission on Radiation Protection
ICRU	International Commission on Radiation Units
MDCT	Multi-Detector Computed Tomography
PA	Pulmonary Angiography
PE	Pulmonary Embolism
UNSCEAR	The United Nation Scientific Committee

List of Contents

Abstract

Radiation exposure associated with multislice CT has increased substantially over the past two decades and is a major concern that needs to quantify the patient doses during Ct procedures. The aim of this study was to evaluate the radiation doses from Chest Computed Tomography Examinations. The data used in this study was collected from Modern Medical Center MMC-Khartoum the data collected from November 2017 to January 2018. A total of 66 patients were examined in CT department with GE machine (Optima) 16 slice. The amount of radiation dose a patient receives from a CT scan depends upon two key factors; the $CTDI_{vol}$ and the DLP.

The result of the study revealed that the values we obtained from CT Chest with contrast exam was $CTDI_{vol}$ 8.69±3.620 mGy, DLP 702.54±344.37 mGy/cm and Effective Dose (ED) was 9.84±4.82 mGy, from HRCT study; $CTDI_{vol}$ was 12.48±3.732 mGy, DLP 387.92±121.48 mGy/cm and ED 5.43±1.70 mGy and from Pulmonary angiography procedure was $CTDI_{vol}$ 13.53±3.20 mGy, DLP 986.73±276.12 mGy/cm and ED 13.81±3.86 mGy

Selection of the most appropriate imaging modality should be performed in view of the delivered doses, required image quality and information and the clinical circumstances.

الخلاصة

التعرض للإشعاع المرتبط بجهاز الأشعة المقطعية متعدد الكواشف قد زاد بشكل كبير على مدى العقدين الماضيين، وهو مصدر قلق كبير يحتاج إلى تحديد جرعة المريض خلال إجراءات فحوصات الأشعة المقطعية.

وكان الهدف من هذه الدراسة تقييم الجرعات الإشعاعية المتلقاة خلال الفحص المقطعي للصدر. تم جمع البيانات المستخدمة في هذه الدراسة من المركز الطبي الحديث بالخرطوم في الفترة من نوفمبر 2017 إلى يناير 2018. تم فحص ما مجموعه 66 مريضا في قسم الأشعة المقطعية بجهاز (GE-OPTIMA) الذي يحتوي علي 16 شريحة.

أظهرت الدراسة أن كمية الجرعة الإشعاعية التي يتلقاها المريض من الأشعة المقطعية تعتمد على عاملين رئيسيين؛ الجرعة الكلية الناتجة عن الفحص ومؤشر الجرعة للشريحة الواحدة. وقد أظهرت نتائج الدراسة أن الجرعة الأشعاعية الناتجة من فحص الصدر بالصبغة كان مؤشر الجرعة 8.69 ± 3.620 ملي قراي و الجرعة الكلية الناتجة عن الفحص 702.54 ± 344.37 ملي قراي / سم والجرعة الفعالة كانت 9.84 ± 4.82 ملي قراي، و من فحص الاشعة المقطعية عالية التباين كان مؤشر الجرعة 12.48 ± 3.732 ملي قراي، و الجرعة الكلية الناتجة عن الفحص 387.92 ± 121.48 ملي قراي / سم و الجرعة الفعالة 5.43 ± 1.70 ملي قراي ومن فحص الاوعية الدموية للرئة كان مؤشر الجرعة 13.53 ± 3.20 ملي قراي و الجرعة الكلية الناتجة عن الفحص 986.73 ± 276.12 ملي قراي / سم و الجرعة الفعالة 13.81 ± 3.86 ملي غراي .

وينبغي أن يتم اختيار طريقة التصوير الأنسب في ضوء الجرعات التي تم تسليمها، جودة الصورة المطلوبة والمعلومات والظروف السريرية.

Chapter one

Introduction

1.1 Introduction

Computed tomography (CT) is an imaging technique which produces a digital topographic image from diagnostic x-ray. In the early 1970s a major innovation was introduced into diagnostic imaging. This innovation, x-ray CT, is recognized today as the most significant single event in medical imaging since the discovery of x-rays (Romans, 2010).

CT is in its fourth decade of clinical use and has proved invaluable as a diagnostic tool for many clinical applications, from cancer diagnosis to trauma to osteoporosis screening. CT was the first imaging modality that made it possible to probe the inner depths of the body, slice by slice. Since 1972, when the first head CT scanner was introduced, CT has matured greatly and gained technological sophistication. Concomitant changes have occurred in the quality of CT images (Seeram, 2015).

CT is one of the many technologies that were made possible by the invention of the computer. The clinical potential of CT became obvious during its early clinical use, and the excitement forever solidified the role of computers in medical imaging. Recent advances in acquisition geometry, detector technology, multiple detector arrays, and x-ray tube design have led to scan times now measured in fractions of a second. Modern computers deliver computational power that allows reconstruction of the image data essentially in real time (Kalender, 2000).

A routine chest protocol includes both soft tissue and lung windows to evaluate mediastinal structures in conjunction with lung tissue. Scans extend from the lung apices to under the diaphragm (including the adrenals when

there is history of certain carcinomas). The administration of IV contrast media is dependent on the clinical indication and the preference of the radiologist. Demarcation of the esophagus can be improved by giving an oral barium suspension shortly before starting the scan (Braun et al., 2015).

CT imaging of the chest presents unique challenges because of the continuous motion of the heart and vascular structures. Improvements in temporal and spatial resolution that have been realized as a result of multidetector-row CT (MDCT) have been particularly valuable in thoracic imaging. This technology allows the entire thorax to be scanned with thin sections during a single breath-hold, making consistent high-resolution imaging possible. Electrocardiographic (ECG) synchronization with MDCT is another valuable tool used to reduce cardiovascular motion artifact and improve image quality. Postprocessing techniques, such as three-dimensional (3D) and multiplanar reformations (MPR) can accurately display the pulmonary and coronary vasculature. These new, noninvasive CT imaging techniques can augment, and sometimes replace, the information provided from more invasive tests such as aortography, pulmonary angiography, and coronary angiography. Despite the enormous benefits presented by newer technologies, not all technical and diagnostic problems have been solved. We continue to struggle to find an ideal compromise between image quality, diagnostic accuracy, and patient radiation dose (Romans, 2010).

Over the years a lot of surveys have been carried out trying to estimate not only the collective dose of computed tomography (CT) examinations but also the effective dose for specific scan regions.

1.2 Problem of the Study

No sufficient previous studies in such subject in Sudan. And the technologists they don't follow the same protocol for the same procedures which makes differences of patient's dose.

1.3 Objective of the study

1.3.1 General Objective

To Estimate of patient dose during Chest examination in Computed Tomography.

1.3.2 Specific Objectives

- To Estimate of patient dose during HRCT
- To Evaluate of patient dose from Pulmonary Angiography
- To Calculate of Effective dose for all patients that undergoes routine Chest CT
- To Compare of the results with international DRLS

1.4 Overview of the Study

This thesis is concerned with assessment of radiation dose at CT Chest and. Accordingly, it is divided into the following chapters:

Chapter one is the introduction, objectives, thesis problem and outline. Chapter two contains the background: literature review, and theoretical concepts of radiation dosimetry and technique. Chapter three describes the materials and methods. Chapter four represents the results of this study. Chapter five present discussion, conclusions and Recommendations.

Chapter Two

Theoretical Background and literature review

2.1 Anatomy of Chest

The thorax is the upper part of the trunk. It consists of an external musculoskeletal cage, the thoracic wall, and an internal cavity that contains the heart, lungs, esophagus, trachea and principal bronchi, thymus, vagus and phrenic nerves, right and left sympathetic trunks, thoracic duct, lymph nodes, and major systemic and pulmonary blood vessels (Ellis, 2007).

Inferiorly, the thorax is separated from the abdominal cavity by the diaphragm; superiorly, it communicates with the neck and the upper limbs.

The thoracic wall offers protection to some of the abdominal viscera: the greater part of the liver lies under the right dome of the diaphragm; the stomach and spleen lie under the left dome of the diaphragm; and the posterior aspects of the superior poles of the kidneys lie on the diaphragm and are anterior to the twelfth rib on the right, and to the eleventh and twelfth ribs on the left (Riquet et al., 2013).

Functionally, the thorax and its encased visceral structures are involved in the following:

Protection: the thoracic cage and its muscles protect the vital structures in the thorax.

Support: the thoracic cage provides muscular support for the upper limb.

Conduit: the thorax provides for a superior and an inferior thoracic aperture and a central mediastinum.

Segmentation: the thorax provides an excellent example of segmentation, a hallmark of the vertebrate body plan.

Breathing: movements of the diaphragm and intercostal muscles are essential for expanding the thoracic cavity to facilitate the entry of air into the lungs in the process of breathing.

Pumping blood: the thorax contains the heart, which pumps blood through the pulmonary and systemic circulations (Clemens et al., 2011).

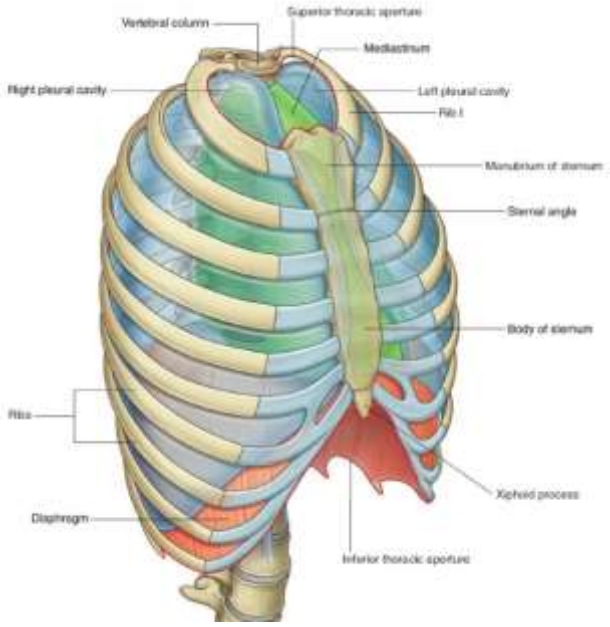

Figure (2.1): Thoracic wall and cavity.

The sternum, ribs (12 pairs), and thoracic vertebrae (12) encircle the thoracic contents and provide a stable thoracic cage that both protects the visceral structures of the thorax and offers assistance with breathing. Because of the lower extent of the rib cage, the thorax also offers protection for some of the abdominal viscera, including the liver and gallbladder on the right side, the stomach and spleen on the left side, and the adrenal (suprarenal) glands and upper poles of the kidneys on both sides (Clemens et al., 2011).

The **superior thoracic aperture** (the anatomical thoracic inlet) conveys large vessels, important nerves, the thoracic lymphatic duct, the trachea, and the esophagus between the neck and thorax (Clemens et al., 2011).

The **inferior thoracic aperture** (the anatomical thoracic outlet) conveys the inferior vena cava (IVC), aorta, esophagus, nerves, and thoracic lymphatic duct between the thorax and the abdominal cavity.

The thorax contains two pleural cavities laterally and a central "middle space" called the mediastinum, which is divided as follows:

Superior mediastinum: a midline compartment that lies above an imaginary horizontal plane that passes through the manubrium of the sternum (sternal angle of Louis) and the intervertebral disc between the T4 and T5 vertebrae.

Inferior mediastinum: the midline compartment below this same horizontal plane, which is further subdivided into an anterior, middle (contains the heart), and posterior mediastinum (Carrier et al., 2007).

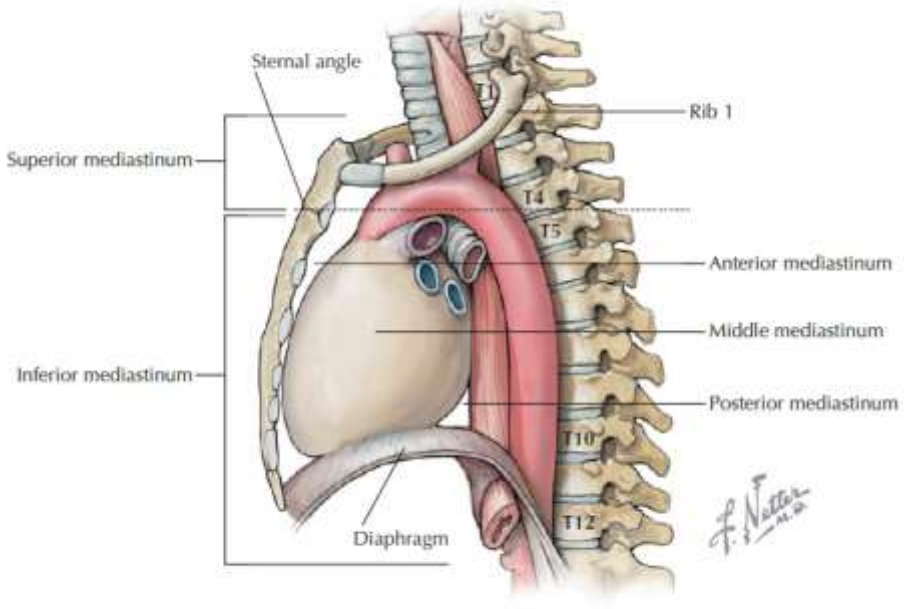

Figure (2.2): Subdivisions of the Mediastinum.

2.1.1 Surface Anatomy:

Jugular (suprasternal) notch: a notch marking the level of the second thoracic vertebra, the top of the manubrium, and the midpoint between the articulations of the two clavicles. The trachea is palpable in the suprasternal notch (Karargyris et al., 2011).

Sternal angle (of Louis): marks the articulation between the manubrium and body of the sternum, the dividing line between the superior and the inferior mediastinum, and the site of articulation of the second ribs (useful for counting ribs and intercostal spaces) (Sussmann and Ko, 2010).

Nipple: marks the T4 dermatome and approximate level of the dome of the diaphragm on the right side (Karargyris et al., 2011).

Xiphoid process: marks the inferior extent of the sternum and the anterior attachment point of the diaphragm.

Thoracic Cage: The **thoracic skeleton** forms the osteocartilaginous *thoracic cage*. The thoracic skeleton includes 12 pairs of ribs and costal cartilages, 12 thoracic vertebrae and intervertebral (IV) discs, and the sternum. Costal cartilages form the anterior continuation of the ribs, providing a flexible attachment at their articulation with the sternum. The ribs and their cartilages are separated by **intercostal spaces**, which are occupied by intercostal muscles, vessels, and nerves (Carrier et al., 2007).

2.2 Protocols of CT Chest Examinations:

Most thoracic protocols are performed while the patient lies in a supine position on the scan table with the arms elevated above the head. In a few instances, primarily high resolution CT protocols of the lungs, additional scans are obtained with the patient in the prone position. Using the shortest scan time possible helps to reduce artifacts created by respiratory motion.

Whenever possible, scans of the chest should be acquired within a single breath-hold, as this will prevent misregistration that may be caused by uneven patient breathing between scans (Mayo et al., 1995).

The thorax has the highest intrinsic natural contrast of any body part. The pulmonary vessels and ribs have significantly different attenuation values compared with the adjacent aerated lung. In most adults, the mediastinal vessels and lymph nodes are surrounded by enough fat to be easily identified. Because of this intrinsic natural contrast, intravenous (IV) iodinated contrast administration is not necessary for all thoracic indications. For example, scans done for the screening, detection, or exclusion of pulmonary nodules or primary lung diseases such as emphysema or fibrosis are typically done without IV contrast administration. The use of IV contrast material is typically requested by the radiologist to differentiate vascular from nonvascular structures, particularly lymph nodes, to evaluate cardiovascular structures by seeing the inside of these structures, and to further characterize lesions by observing their pattern of enhancement.

The demarcation of the esophagus and the gastroesophageal junction can be improved by giving the patient an oral contrast agent, most often a barium suspension, shortly before beginning the scan, but is not necessary for most thoracic CT examinations (Kalender, 2000).

2.2.1 CT of the Airways

Technical parameters used for CT imaging of the airways include the use of thin sections (1.25 mm or less), a fast acquisition that allows the entire lungs to be scanned during a single breath-hold, optimal spatial resolution, and the use of postprocessing techniques. Overlapping *z* axis image reconstruction of 50% is typical. Neither IV nor oral contrast media are routinely required; IV contrast may be used in cases of airway tumors (Singh et al., 2011).

Airway imaging is routinely performed at both inspiration and expiration. CT is generally accepted as the best imaging technique for assessment of disease of the central airways1 and is most commonly used to look for narrowing that may occur in patients who have been intubated in the past. Applying postprocessing techniques, such as volume rendering, may be referred to as CT bronchography. Virtual bronchoscopy is accomplished with similar postprocessing techniques, but is different in that it offers an internal rendering of the tracheobronchial walls and lumen (Romans, 2010).

2.2.2 High-resolution CT (HRCT)

High-resolution CT (HRCT) is used to evaluate the lung parenchyma in patients with known or suspected diffuse lung diseases such as fibrosis and emphysema. Like airway imaging, HRCT protocols use thin sections (1.5 mm or less), a fast acquisition to reduce motion artifact, and optimal spatial resolution. In addition to the thin sections, spatial resolution is optimized by the selection of an edge-enhancing algorithm (such as a bone algorithm) and a display field of view (DFOV) that is just large enough to include the lungs. In some institutions, HRCT protocols are incremental, meaning images are obtained with an interval of 10 mm or more between slices and only approximately 10% of the lung parenchyma is scanned. This technique is intended to provide representative areas of lung disease. However, because evidence of some types of diffuse lung disease may not be uniform in distribution throughout the lung, this method of sampling may result in characteristic foci of the disease not being imaged (Mayo et al., 1993).

More recently, as MDCT scanners have become commonplace, the technique known as volumetric. HRCT is replacing the HRCT axial protocols. Volumetric HRCT protocols use a helical mode to acquire images of the entire lung, rather than representative slices. Because these helical

protocols cover the entire lung, they result in a more complete assessment of the lung. Lung nodules that could be missed between slices in incremental protocols are not missed with volumetric HRCT, and the central airways can be evaluated at the same time. In addition, they allow postprocessing techniques such as maximum (MIP) and minimum (MinIP) intensity projection reformation. Although there are clear advantages to the use of volumetric HRCT over an interspaced technique, the increased radiation exposure is a consideration. Many volumetric HRCT protocols decrease the tube current (mA) to reduce the radiation dose (Mettler Jr et al., 2000).

Many HRCT protocols (both volumetric and axial) include more than one series of scans. In all patients there is a gradual increase in attenuation and vessel size from anterior to posterior lung regions owing to the effect of gravity on blood flow and gas volume. In addition, there can be atelectasis in the most dependent lung (i.e., the side touching the CT table) that can mimic or hide lung disease. An additional series of prone images can help to differentiate actual disease from what is not. Expiratory scans are used to look for areas of the lung that do not empty or get smaller, which indicates small airway disease. When the lungs are fully expanded the contrast between low-attenuation aerated air space and high-attenuation lung structure is maximized (Lauri, 2017).

Therefore, HRCT protocols are routinely obtained at full inspiration. However, expiratory images are useful in many instances. For example, expiratory images better depict bronchiolitis and air trapping. The density gradient from the effects of gravity is more pronounced on expiratory images. For these reasons, HRCT protocols may include three series of scans: inspiratory supine, expiratory supine and inspiratory prone. In volumetric protocols, only the inspiratory supine series is done in a helical

mode. The additional images are done in the representative axial fashion to reduce the radiation exposure (Lauri, 2017).

2.2.3 THORACIC CTA

The MDCT advantages of high temporal and spatial resolution are particularly well suited to accurately image the heart and thoracic vessels, and have resulted in many new scanning protocols. The following discussion of the use of MDCT in the diagnosis of pulmonary embolism explores many of the issues that must be addressed in CT angiography (CTA) examinations of the thorax. However, the detection of pulmonary embolism is just one of many indications for chest CTA (Zhi et al., 2017).

MDCT angiography has become an imaging mainstay in the diagnosis of pulmonary embolism (PE). MDCT scanners have energized this trend with improved image quality, thinner slices to promote enhanced postprocessing reconstruction, superb CT angiographic capability, and more rapid imaging to assist in scanning the dyspneic patient. CT pulmonary angiography is considered by many to be better than traditional catheter or invasive pulmonary angiography, which is limited in the number of projections and suffers from vessel overlap (Ramjattan and Makaryus, 2017).

To assist the technologist in understanding the role of CT in the diagnosis of PE we start with a review of the basic medical terminology and anatomy relating to the pulmonary circulation. We then look briefly at the strengths and limitations of other common diagnostic options. Finally, we examine the specific parameters that make up a PE protocol (Seeram, 2015).

2.3 CT Parameters for Influence the Radiation Dose

The exposure to radiation of patients undergoing computed tomography (CT) examinations is determined by two factors: equipment-related factors, i.e., design of the scanner with respect to dose efficiency, and application-

related factors, i.e., the way in which the radiologist or the radiographer makes use of the scanner. In this chapter, the features and parameters influencing patient dose are outlined. First, however, a brief introduction on the dose descriptors applicable to CT is given (Zhu et al., 2004).

2.3.1 CT Dose Descriptors

The dose quantities used in projection radiography are not applicable to CT for three reasons; First, the dose distribution inside the patient is completely different from that for a conventional radiogram, where the dose decreases continuously from the entrance of the X-ray beam to its exit, with a ratio of between 100 and 1000 to 1. In the case of CT, as a consequence of the scanning procedure that equally irradiates the patient from all directions, the dose is almost equally distributed in the scanning plane. A dose comparison of CT with conventional projection radiography in terms of skin dose therefore does not make any sense (Mayo et al., 2004).

Second, the scanning procedure using narrow beams along the longitudinal z-axis of the patient implies that a significant portion of the radiation energy is deposited outside the nominal beam width. This is mainly due to penumbra effects and scattered radiation produced inside the beam (Mayo et al., 2004). Third, the situation with CT–unlike with conventional projection radiography–is further complicated by the circumstances in which the volume to be imaged is not irradiated simultaneously. This often leads to confusion about what the dose from a complete series of, for example, 15 slices might be compared with the dose from a single slice (Mayo et al., 2004).

As a consequence, dedicated dose quantities that account for these peculiarities are needed: the ‘computed tomography dose index (CTDI)’, which is a measure of the local dose, and the ‘dose–length product (DLP)’,

representing the integral radiation exposure associated with a CT examination. Fortunately, a bridge exists that enables comparison of CT with radiation exposure from other modalities and sources; this can be achieved by the effective dose (E). So, there are three dose descriptors in all, which everyone dealing with CT should be familiar with (Parker et al., 2008).

2.3.2Computed Tomography Dose Index

The CTDI is the fundamental CT dose descriptor. By making use of this quantity, the first two peculiarities of CT scanning are taken into account: The CTDI [unit: milligray (mGy)] is derived from the dose distribution along a line that is parallel to the axis of rotation for the scanner (= z-axis) and is recorded for a single rotation of the X-ray source (Livingstone et al., 2010).

(Figure 2.10) illustrates the meaning of this term: CTDI is the equivalent of the dose value inside the irradiated slice (beam) that would result if the absorbed radiation dose profile were entirely concentrated to a rectangular profile of width equal to the nominal beam width N.hcol, with N being the number of independent (i.e., non-overlapping) slices that are acquired simultaneously. Accordingly, all dose contributions from outside the nominal beam width, i.e., the areas under the tails of the dose profile, are added to the area inside the slice (Zanca et al., 2012).

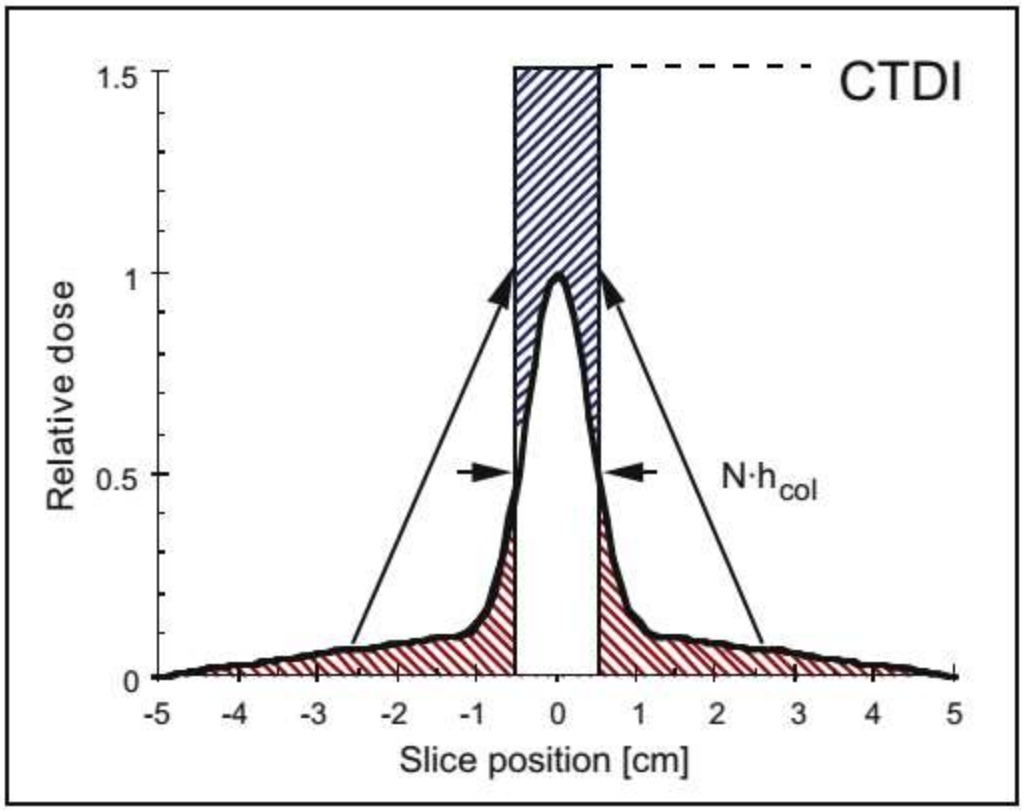

Figure (2.3) Illustration of the term 'Computed Tomography Dose Index (CTDI)': CTDI is the equivalent of the dose value inside the irradiated slice (beam) that would result if the absorbed radiation dose profile were entirely concentrated to a rectangular profile of width equal to the nominal beam width $N.h_{col}$

The corresponding mathematical definition of CTDI therefore describes the summation of all dose contributions along the z-axis:

$$CTDI = \frac{1}{N \cdot h_{col}} \cdot \int_{-}^{+} D(z) \cdot dz \qquad 2.2$$

Where D(z) is the value of the dose at a given location, z, and $N.h_{col}$ is the nominal value of the total collimation (beam width) that is used for data acquisition. CTDI is therefore equal to the area of the dose profile (the 'dose–profile integral') divided by the nominal beam width. In practice, the

dose profile is accumulated in a range of -50 mm to +50 mm relative to the center of the beam, i.e., over a distance of 100 mm (Zanca et al., 2012).

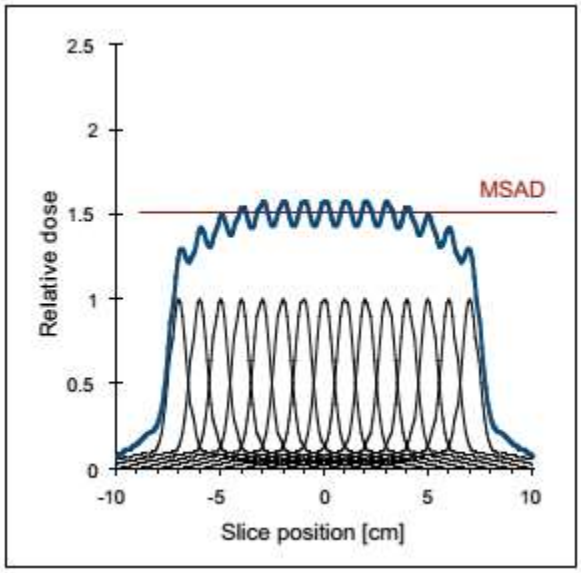

Figure (2.11): Total dose profile of a scan series with n=15 subsequent rotations. The average level of the total dose profile, which is called 'Multiple Scan Average Dose (MSAD)', is equal to the computed tomography dose index (CTDI) if the table feed (TF) is equal to the nominal beam width $N.h_{col}$ (i.e., pitch p = 1)

The relevance of CTDI becomes obvious from the total dose profile of a scan series with, for example, n = 15 subsequent rotations (Fig. 4.2). The average level of the total dose profile, which is called 'multiple scan average dose (MSAD)' (Shope1981), is higher than the peak value of each single dose profile. This increase results from the tails of the single dose profiles for a scan series. Obviously, MSAD and CTDI are exactly equal if the table feed (TF) is equal to the nominal beam width $N.h_{col,}$ i.e., if the pitch factor

$$p = \frac{TF}{N \cdot h_{col}} \qquad 2.3$$

Is equal to 1. In general (i.e., if the pitch is not equal to 1, Fig. 2.12), the relationship between CTDI and MSAD is given by

$$MSAD = \frac{1}{p} \cdot CTDI \qquad 2.4$$

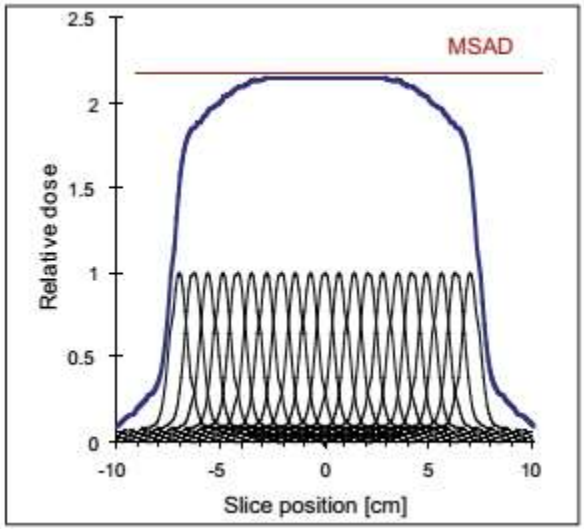

Figure (2.12): Total dose profile of a scan series with n = 15 subsequent rotations, although scanned with pitch = 0.7. Due to the larger overlap, multiple scan average dose (MSAD) is higher than that in Fig. 4.2 and amounts to computed tomography dose index (CTDI) divided by pitch

The practical implication of Equation 2.4 is that, in order to obtain the average dose for a scan series, it is not necessary to carry out all the scans. Instead, it is sufficient to obtain the CTDI from a single scan by acquiring the entire dose profile according to Equation 4.1. This is achieved with dose measurements using long, pencil-like detectors, with an active length of 10 cm (Fig. 4.4). These detectors accumulate the dose profile integral (DPI; unit: mGy.cm).

The CTDI is then obtained according to Equation 4.1 by dividing by the nominal beam width $N.h_{col}$. In order to obtain estimates of the dose to organs located in the scan range, the CTDI generally refers to standard dosimetry phantoms with patient-like diameters. In the standard measuring procedure for CTDI, which utilizes two cylindrical Perspex (PMMA) phantoms of different diameter (Fig. 2.13), dose is measured at the center and near the periphery of the phantom (Fig. 2.14). The larger phantom, being 32 cm in diameter, represents the absorption that is typical for the trunk region of adults. The smaller phantom (16 cm in diameter) represents the patient in head examinations. The smaller phantom is also used for dose assessment in pediatric examinations (Singh et al., 2011). The dose values thus obtained are denoted as:

$$CTDI_{H,c} \text{ and } CTDI_{H,p}$$

and

$$CTDI_{B,c} \text{ and } CTDI_{B,p}$$

With H = head, B = body, c = center, p = periphery.

To make life easier, each pair of CTDI values (central and peripheral) can be combined into a single one named 'weighted CTDI ($CTDI_w$)', which represents the CTDI averaged over the cross section of the pertaining phantom

$$CTDI_W = \frac{1}{3} \cdot CTDI_{XYZ,c} + \frac{2}{3} \cdot CTDI_{XYZ,p} \qquad 2.4$$

Where the subscript XYZ stands for either H(ead) or B(ody). In daily practice, CTDIw is used as one of two dose descriptors for dose recommendations ('reference values') that have been introduced by the European Commission (1999a)

Figure (2.13) Cylindrical standard computed tomography (CT) dosimetry phantoms (16 cm and 32 cm in diameter) made from Perspex for representative measurements of the computed tomography dose index (CTDI) in regions of the head and the trunk, and a pencil-like detector for measurements of the dose-profile integral

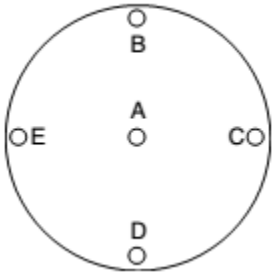

Figure (2.14): Arrangement of the locations A–E for the determination of the computed tomography dose index (CTDI) in a standard CT dosimetry phantom If pitch-related effects on the radiation exposure have already been taken into account at the level of local dose (i.e., CTDI), a quantity named 'volume

CTDI ($CTDI_{vol}$)' is defined (IEC 2001):

$$CTDI_{vol} = \frac{CTDI_w}{p} \qquad 2.5$$

So CTDIvol is the pitch-corrected CTDI w. Apart from the integration length, which is limited to 100 mm, $CTDI_{vol}$ is practically identical to MSAD based on $CTDI_w$ (i.e., MSAD $_w$). Since averaging includes both the cross section and the scan length, CTDIvol therefore represents the average dose for a given scan volume. CTDIvol is used as the dose quantity that is displayed at the operator's console of newer scanners. This also holds true even if the display is labeled as 'CTDIw' due to faulty definition in the first edition of the particular IEC standard for CT (IEC 1999), or simply as 'CTDI'.

Attention is required if the dose displayed as CTDIvol shall be used for comparison with reference values given in terms of CTDIw. For this purpose, the pitch correction introduced in Equation 2.6 needs to be reversed by multiplying the CTDIvol value by the pitch factor. Care is also required if the CTDIvol displayed is used to assess pediatric radiation exposure: whether head or body CTDI values are displayed depends only on the scan mode (head or body), not on the patient size. Consequently, the dose to children and infants undergoing CT examinations of the trunk region, which for the same scan parameter settings depends on the patient diameter, is currently underestimated with the dose displayed at the operator's console by a factor two to three (Singh et al., 2013).

CTDI statements in scanner specification sheets are given for the head phantom as well as for the body phantom and often apply to a current–time product of 100 mAs or 1 mAs. In this case, it must be recognized that a quantity named 'normalized CTDI' is used, which is labeled 'n CTDI (unit:

mGy/mAs)' in order to avoid confusion. The normalized CTDI is obtained by dividing the CTDI value by the mAs product Q that was used to measure CTDI:

$$_{n}CTDI = \frac{CTDI}{Q} \qquad 2.6$$

It is worthwhile (and indeed necessary) to note that the normalized CTDI is a characteristic quantity for a scanner (dose rate coefficient), which simply represents the capacity of a scanner in terms of output and conveys absolutely nothing about patient dose. Very often it is assumed that scanners with a high value of $_{n}$CTDI are more 'dangerous' than other models with lower $_{n}$CTDI values. This is not necessarily the case. Reference to patient dose cannot be made unless the normalized CTDI has been multiplied by the tube current–time product Q that is required in order to produce images of diagnostic quality with the type of scanner under consideration. Only after having carried out this step is it possible to decide whether a particular scanner needs more or less dose than another model for a specified type of examination (Chae et al., 2014).

2.3.3 Dose–Length Product

The third peculiarity of CT, i.e., the question of what the dose from a complete series of, for example, 15 slices might be compared with that from a single slice, is solved by introducing a dose descriptor named 'dose–length product (DLP; unit: mGy.cm)'.

DLP takes both the 'intensity' (represented by the $CTDI_{vol}$) and the extension (represented by the scan length L) of an irradiation into account (Fig. 2.15)

$$DLP = CTDI_{vol} \cdot L \qquad 2.7$$

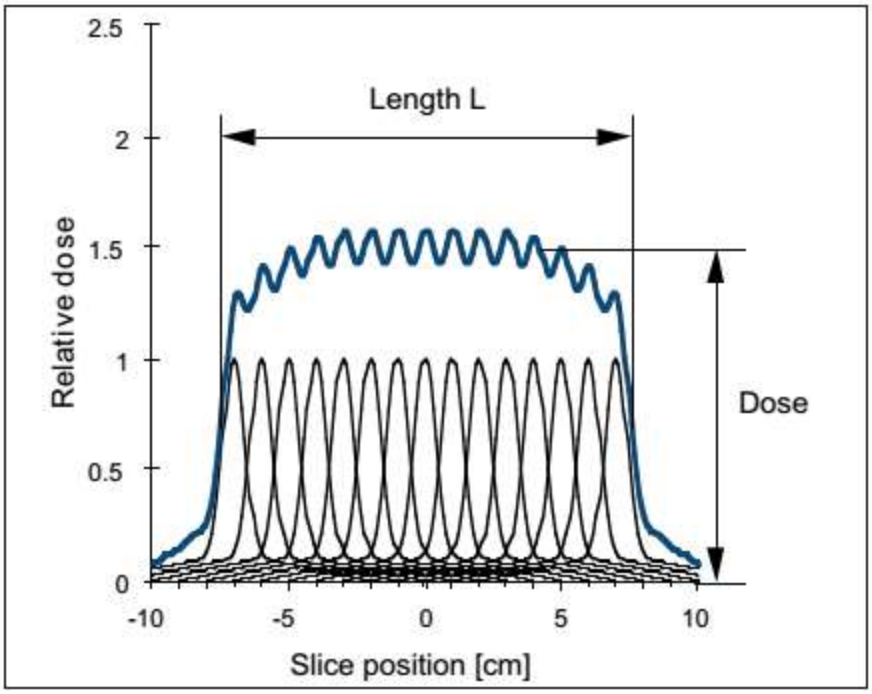

Figure (2.15): Total dose profile of a scan series with n=15 subsequent rotations. The dose–length product (DLP) is the product of the height ($CTDI_{vol}$) and the width (scan length L) of the total dose profile and is equal to the area under the curve

So the DLP increases with the number of slices (correctly: with the length of the irradiated body section), while the dose (i.e., $CTDI_{vol}$) remains the same regardless of the number of slices or length (Gabusi et al., 2016).

In Figure 4.15, the area of the total dose profile of the scan series represents the DLP. DLP is the equivalent of the dose–area product (DAP) in projection radiography, a quantity that also combines both aspects (intensity and extension) of patient exposure (Gabusi et al., 2016).

In sequential scanning, the scan length is determined by the beam width $N.h_{col}$ and the number (n) of table feeds (TF)

$$L = n \cdot TF + N \cdot h_{col} \qquad 2.8$$

While in spiral scanning the scan length only depends on the number (n) of rotations and the table feed (TF)

$$L = n \cdot TF = \frac{T}{t_{rot}} \cdot p \cdot N \cdot h_{col} \qquad 2.9$$

Where T is the total scan time, t_{rot} is the rotation time, and p is the pitch factor. While in sequential scanning the scan length L is equal to the range from the beginning of the first slice until the end of the last, the (gross) scan length for spiral scanning not only comprises the (net) length of the imaged body section but also includes the additional rotations at the beginning and the end of the scan ('overranging') which are required for data interpolation. If an examination consists of several sequential scan series or spiral scans, the DLP of the complete examination (DLP_{exam}) is the sum of the DLPs of each single series or spiral scan (Macia-Suarez et al., 2017).

$$DLP_{exam} = \sum_i DLP_i \qquad 2.10$$

In daily practice, the DLP is used as the second (and most important) of the two dose descriptors for dose recommendations ('reference values') that have been introduced by the European Commission (1999a).

2.3.4 Effective Dose

CTDI and DLP are CT-specific dose descriptors that do not allow for comparisons with radiation exposures from other sources, e.g., projection radiography, nuclear medicine or natural background radiation. The only common denominator to achieve this goal is the 'effective dose'.

With effective dose, the organ doses from a partial irradiation of the body are converted into an equivalent uniform dose to the entire body (Braun et al., 2015).

Effective dose E [unit: millisievert (mSv)] according to ICRP 60 (ICRP 991) is defined as the weighted average of organ dose values HT for a number of specified organs:

$$E = \sum_i w_i \cdot H_{T,i} \qquad 2.11$$

Effective dose cannot as such be measured directly in vivo. Measurements in anthropomorphic phantoms with thermo-luminescent dosemeters (TLDs) are very time-consuming and therefore not well suited for daily practice. Effective dose, however, can be assessed in various ways using conversion factors.

For coarse estimates, it is sufficient to multiply the DLP with mean conversion factors, depending on which one of three body regions has been scanned and whether that scan was made in head or body scanning mode:

$$E \approx DLP \cdot f_{mean} \qquad 2.12$$

For adults of standard size, the following generic mean conversion factors f_{mean} apply:

1. 0.025 mSv/mGy.cm for the head region
2. 0.060 mSv/mGy.cm for the neck region, scanned in head mode
3. 0.100 mSv/mGy.cm for the neck region, scanned in body mode
4. 0.175 mSv/mGy.cm for the trunk region

Similar factors ('E_{DLP}'), which additionally distinguish between chest, abdomen and pelvis, but do not account for differences in scan mode, are given in report EUR 16262 (European Commission 1999b).

In order to apply Equation 4.13, the DLP or at least the $CTDI_{vol}$ and the (gross) scan length L, from which the DLP can be calculated according to

Equation 2.12, must be available. If the scanner is not equipped with a dose display, or if a more detailed assessment of effective dose is desired (e.g., to be more specific for the scanned region of the body, to distinguish between males and females, to assess pediatric doses, or to take differences between scanners into account), dedicated CT dose calculation software should be used. These programs make use of more detailed conversion factors and also allow for calculation of organ doses. Currently, five different programs are in general use. They are available either commercially or as freeware and differ significantly in specifications, performance, and price (Braun et al., 2015).

Typical tolerances in effective dose assessment with these programs are in the order of ±20–30%.

Similar uncertainties also apply to effective dose assessment with TLD measurements in Alderson phantoms. This should always be borne in mind when comparing doses from different scanners in terms of effective dose. Care is also needed not to mix up effective dose with organ doses, as both are expressed in millisieverts. Nevertheless, effective dose is of great value, e.g., to answer questions raised by patients. For this purpose, the annual natural background radiation, which is between 2 mSv and 3 mSv in most countries, can be used as a scale (Protection, 1999).

A comprehensive compilation of dose-relevant scanner data and other useful information required for CT dose assessment can be found in a textbook by (Nagel et.al, 2002). The data given there apply to most of the scanners currently in use, except the most recent. However, data for these new scanners can be found in the CT-Expo software package, which is based on the data and formalism outlined in this book and is updated regularly (Stamm and Nagel, 2002).

2.4 CT radiation risk

CT scans use a high level of ionizing radiation. Ionizing radiation has the capacity to break molecular bonds, and thus alter the molecular structure of the irradiated molecules. The human body cells operation is controlled by the chemical structure of the DNA molecule that they include. Ionizing radiation cause DNA double strand breaks at a rate of 35 double strand breaks per cell per Gray, and removes a portion of the epigenetic markers of the DNA, which regulate the gene expression. At the radiation doses, which typical CT scans impose, a DNA molecule of 40%-100% of the irradiated cells is damaged by one or more double strand breaks. This insult is followed by an effort of the cell in attempt to repair the damaged and broken DNA, however, the repair process is not perfect and faults that are not properly repaired can cause the cell to stray from its original design of operation. The improper operation can manifest in cell death, cancer, and in other puzzling health conditions, as can be expected from an operation, which randomly alter cell's DNA, and epigenetic markers. (Roxanne Nelson 2009) A portion of the population possess a flawed DNA repair mechanism, and thus suffer a greater insult due to exposure to radiation Unlike CT, MRI does not use ionizing radiation, and does not cause double strand breaks to the DNA (Li et al., 2011).

The individual risk from radiation associated with a CT scan is quite small compared to the benefits that accurate diagnoses and treatment can prove. Still, unnecessary radiation exposure during medical procedures should be avoided. Unnecessary radiation may be delivered when CT scanner parameters are not appropriate adjusted for the patient size (de Margerie-Mellon et al., 2016).

There is no doubt that many patient have benefited from the rapid diagnoses made possible by CT and from its value for monitoring chronic disease. However is increasing concern regarding the risk of this exposure to radiation. It is well established that radiation can be harmful and has both deterministic and stochastic effects. Deterministic effect, such as hair loss, skin burns, and cell death, are dose dependent but do not occur below a threshold of 150-200 mSv. Since the typical estimated dose associated with proper use of CT is in the range of 2-10 mSv, deterministic effects are not normally a concern. Induction of cancer by radiation is a probabilistic (stochastic) effect, not a deterministic effect. That is, higher radiation doses are associated with a higher likelihood of carcinogenesis, but even low doses of radiation could potentially induce carcinogenesis and it is more difficult to assess a safe level of exposure (Larke et al., 2011).

CT was always considered a “high dose” technique, there is growing realization that image quality in CT often exceeds the level needed for confident diagnosis and that patient doses are higher than necessary (Mettler Jr et al., 2000).

In conventional X-ray procedure, medical personnel can tell if the patient has been overexposed because of the film is overexposed, produce a dark image (ICRP 2006). However, with CT there is no obvious evidence that the patient has been overexposed because the quality of the image may not be compromised. Several recent articles (Zhu et al., 2004, Mayo et al., 2004, Parker et al., 2008) stress that is important to use the lowest radiation dose necessary to provide an image from which an accurate diagnosis can be made, and that signification dose reduction can be achieved without compromising clinical efficacy (Mettler Jr et al., 2000).

The United Nation Scientific Committee on the Effects of Atomic Radiation (UNSCEAR, 2000) has highlighted that the worldwide there about 93 million CT examination performed annually at a rate of about 57 examination per 1000 persons. UNSCEAR also estimated that CT constitutes about 5% of all X-ray examination worldwide will accounting for about 34% of the resultant collective dose. In the countries that were identified as having the highest levels of healthcare, the corresponding figures were 6% and 41% respectively. New advancement of the CT has also led to great increase of the radiation dose to the patients. The use of multi-slice computed tomography (MSCT) has aggravated the scenario with the increasing of collective dose of CT examinations because the MSCT produces higher dose to the patients compared to single slice CT (SSCT) (Lim et al., 2016).

2.5 Previous studies:

Tomasz Gorycki et al, 2014 discussed the reference diagnostic levels for the computed tomography (CT) of the chest as cited in different literature sources. The doses was expressed either in weighted CT dose index ($CTDI_{VOL}$) used to express the dose per slice, dose-length product (DLP), and effective dose (E).

The purpose of his study was to assess the radiation dose used in Low Dose Computer Tomography (LDCT) of the chest in comparison with routine chest CT examinations as well as to compare doses delivered in low dose chest CT with chest X-ray doses.

Mean values of $CTDI_{VOL}$ and DLP were, respectively: 2.1 mGy and 85.1 mGy·cm, for low dose, 9.7 mGy and 392.3 mGy·cm for helical, 18.2 mGy

and 813.9 mGy·cm for angio CT, 2.3 mGy and 64.4 mGy·cm for high resolution CT, 8.9 mGy. And 317.6 mGy·cm for helical ASIR protocols.

Significantly lower $CTDI_{VOL}$ and DLP values were observed for low dose and high resolution CT versus the remaining CT protocols; doses delivered in CT ASIR protocols were also lower (80–81%). The ratio between medial doses in low dose CT and chest X-ray was 11.56.

M. Alkhorayef et al, 2017 studied that the Computed tomography angiography (CTA) has become the most valuable imaging modality for the diagnosis of blood vessel diseases; however, patients are exposed to high radiation doses and the probability of cancer and other biological effects is increased. The objectives of this study were to measure the patient radiation dose during a CTA procedure and to estimate the radiation dose and biological effects.

The study was conducted in two radiology departments equipped with 64-slice CT machines (Aquilion) calibrated according to international protocols. A total of 152 patients underwent brain, lower limb, chest, abdomen, and pelvis examinations. The effective radiation dose was estimated using ImPACT scan software. Cancer and biological risks were estimated using the International Commission on Radiological Protection (ICRP) conversion factors.

The mean patient dose value per procedure (dose length product [DLP], mGy.cm) for all examinations was 437.8± 166, 568.8± 194, 516.0± 228, 581.8± 175, and 1082.9± 290 for the lower limbs, pelvis, abdomen, chest, and cerebral, respectively. The lens of the eye, uterus, and ovaries received high radiation doses compared to thyroid and testis.

G Breiki, et al, 2008 found that the CT is responsible for higher doses to patients.

The aim of this work is to study the CT practice in some CT units in different hospitals in Egypt, in order to investigate the radiation doses imparted to patients during CT examinations and image quality.

Dose measurements were performed for the most common applied CT examinations covering radiation sensitive organs in the head and trunk regions.

Selected CT examinations are; routine head, routine chest, routine abdomen and routine pelvis.

Computed Tomography Dose Index (CTDI) was calculated for each scanner from an average of three measurements in the head phantom and another three measurements in the body phantom. DLP values were estimated for each type of examination. Mean values of CTDIw had a range of 36.0-69.0 mGy for head and 11.0-30.0 mGy for chest, abdomen and pelvis examinations.

Organ dose and hence effective dose, calculated using Monte Carlo simulation technique. The effects of selecting tube KV and mAs on both spatial resolution and low contrast detectability were examined for two groups of KV values (90 and 120), the mAs values were degraded from 100 to 300 mAs in 100 mAs interval in first case, and from 50 to 300mAs, in 50mAs interval in second case.

Livingstone et al, 2010 studied that the Radiation doses during chest examinations using dose modulation techniques in multislice CT scanner". The purpose of this study was to evaluate the radiation dose and image quality using a manual protocol and dose modulation techniques in a 6-slice

CT scanner. Two hundred and twenty-one patients who underwent contrast-enhanced CT of the chest were included in the study. For the manual protocol settings, constant tube potential (kV) and tube current-time product (mAs) of 140 kV and 120 mAs, respectively, were used. The angular and z-axis dose modulation techniques utilized a constant tube potential of 140 kV; mAs values were automatically selected by the machine. Effective doses were calculated using dose- length product (DLP) values and the image quality was assessed using the signal-to- noise (SNR) ratio values. Mean effective doses using manual protocol for patients of weights 40-60 kg, 61-80 kg, and 81 kg and above were 8.58mSv, 8.54 mSv, and 9.07 mSv, respectively. Mean effective doses using z-axis dose modulation for patients of weights 40-60 kg, 61-80 kg, and 81 kg and above were 4.95 mSv, 6.87 mSv, and 10.24 mSv, respectively. The SNR at the region of the liver for patients of body weight of 40- 60 kg was 5.1 H, 6.2 H, and 8.8 H for manual, angular, and z-axis dose modulation, respectively. Dose reduction of up to 15% was achieved using angular dose modulation and of up to 42% using z-axis dose modulation, with acceptable diagnostic image quality compared to the manual protocol.

Eltahir Suha, 2008 discussed that the use of CT in medical diagnosis delivers radiation doses to patients that are higher than those from other radiological procedures. Lack of optimized protocols could be an additional source of increased dose in developing countries. The aims of this study are, first, to measure patient doses during CT chest and abdomen procedures, second, to estimate the radiation dose to the breast, and third, to quantify the radiation risks during the procedures.

Patient doses from two common CT examinations were obtained from four hospitals in Khartoum. The patient doses were estimated using measurements of CT dose indexes (CTDI), exposure-related parameters, and the ImPACT spreadsheet based on NRPB conversion factors. A large variation of mean organ doses among hospitals was observed for similar CT examinations. These variations largely originated from different CT scanning protocols used in different hospitals and scanner type. The largest range was found for CT of the chest, for which the dose varied from 2.3 to 47 (average 24.7) mSv and for abdomen CT, it was 1.6 to 18.8 (average 10.2) mSv. Radiation dose to the breast ranged froml.6 to 32.9 mSv for the chest and 1.1 to 13.2 mSv for the abdomen. The radiation risk per procedure was high. The obtained values were mostly higher than the values of organ doses reported from the other studies. It was concluded that current clinical chest and abdomen protocols result in variable radiation doses to the breast. The magnitude of exposure may have implications for imaging strategies.

Justin E., 2006 found that the use of CT in medical diagnosis delivers radiation doses to patients that are higher than those from other radiological procedures, lack of optimized protocols could be an additional source of increased dose in developing countries.

The aims of this study are, first, to determine the magnitude of radiation doses received by selected radiosensitive organs of patients undergoing CT examinations and compare them with other studies, and second, to assess how CT scanning protocols in practice affect patient organ doses. In order to achieve these objectives, patient organ doses from five common CT examinations were obtained from eight hospitals in Tanzania. The patient organ doses were estimated using measurements of CT dose indexes

(CTDI), exposure-related parameters, and the ImPACT spreadsheet based on NRPB conversion factors. A large variation of mean organ doses among hospitals was observed for similar CT examinations. These variations largely originated from different CT scanning protocols used in different hospitals and scanner type. The mean organ doses in this study for the eye lens (for head), thyroid (for chest), breast (for chest), stomach (for abdomen), and ovary (for pelvis) were 63.9 mGy, 12.3 mGy, 26.1 mGy, 35.6 mGy, and 24.0 mGy, respectively.

These values were mostly comparable to and slightly higher than the values of organ doses reported from the literature for the United Kingdom, Japan, Germany, Norway, and the Netherlands. It was concluded that patient organ doses could be substantially minimized through careful selection of scanning parameters based on clinical indications of study, patient size, and body region being examined.

Additional dose reduction to superficial organs would require the use of shielding materials.

Chapter Three

3. Materials and Method

3.1 Area and duration of the study:

The aim of this study was to evaluate the radiation doses from different CT Chest imaging investigations (CT Chest, HRCT and, Pulmonary Angiography). The data used in this study was collected from Modern Medical Center the data collected from November 2017 to January 2018.

3.2 CT machines

CT machine was used to collect data during this study. This machine is installed in radiological department. All quality control tests were performed to the machine prior any data collection. The tests were carried out by experts from Sudan Atomic Energy Commission (SAEC). All the data were within acceptable range. Its specifications were as follows

Manufacturer	Model	Installation	No. of Detectors
General Electric	Optima	2017	16 slice

3.3 Subjects:

The study includes 66 patients (28 male, 38 female) underwent different CT chest examinations (26 CT chest with contrast, 25 HRCT and 15 pulmonary angiography (PA).

3.4 Technique used:

Routine Chest	
Scouts:	AP and lateral
Scan type:	Helical
Start location:	Just above lung apices
End location:	Just below costophrenic angles
Breath-hold:	Inspiration
IV contrast:	80 mL at 3.0 mL/s. 50 mL saline flush. Scan delay = 35 seconds

DFOV:	~38 cm (optimize for individual)
SFOV:	Large body
Algorithm:	Standard
Window settings:	350 ww/50 wl (soft tissue); 1500 ww/−700 wl (lung)
Gantry rotation time	0.8 s
Acquisition (detector width × number of detector rows = detector coverage)	16 × 1.25 = 20 mm
Reconstruction (slice thickness/interval)	2.5 mm/1.25
Pitch	1.375
kVp	120
mA	Auto: min 100/max 150 (noise index 15)

High-Resolution Chest CT	
Scouts:	AP and lateral
Scan type:	Helical
Start location:	Just above lung apices
End location:	Just below costophrenic angles
Breath-hold:	Inspiration
IV contrast:	None
DFOV:	~38 cm (optimize for individual)
SFOV:	Large body
Algorithm:	Bone
Window settings:	1500 ww/−700 wl (lung)
Gantry rotation time	0.5 s
Acquisition (detector width × number of detector rows = detector coverage)	16 × 0.625 = 10 mm
Reconstruction (slice thickness/interval)	1.25 mm/1.25 mm
Pitch	1.375
kVp	140
mA	150-375

CTA-Chest for Pulmonary Embolism	
Scouts:	AP and lateral
Scan type:	Helical
Start location:	Just below lowest hemidiaphragm
End location:	Lung apices
Breath-hold:	Instruct patient to stop breathing (avoid deep inspiration)
IV contrast:	120 mL (370 concentration) total, split bolus; 70 mL at 4.0 mL/s. Scan delay = Smart Prep; set monitor location at the level of the main pulmonary artery, initiate the scan at first sight of contrast

	in the main pulmonary artery (~70 HU); 25-second pause after first 70-mL injection is complete, then 50 mL at 3 mL/s
DFOV:	~38 cm (optimize for individual)
SFOV:	Large body
Algorithm:	Standard
Window settings:	700 ww/180 wl (vascular)
Gantry rotation time	0.5 s
Acquisition (detector width × number of detector rows = detector coverage)	16 × 1.0 = 16 mm
Reconstruction (slice thickness/interval)	1.25 mm/0.625 mm
Pitch	1.375
kVp	120
mA	500

3.4 Data Collection

Data were collected using a sheet for all patients in order to maintain consistency of the information from display (Appendix 1). A data collection sheet was designed to evaluate the patient doses and the radiation related factor. The collected data included, sex, age, tube voltage, tube current–time product settings, pitch; slice thickness, number of slices and turn.

In addition, all scanning parameters were recorded as well as the CT dose descriptors CT volume dose index (in milli Sievert) and dose-length product (in milli Sievert-centimeters).

3.5 Analysis of Data

All dose parameters where registered down and from the display monitor in 16 slice CT scan and they were used in calculation for the effective dose using conversion factor to the chest, then used as input to the statistical software (SPSS) and Microsoft Excel for analysis.

Chapter Four

4. Results

Table (4.1): shows statistical parameters for all patients

	Mean	Median	STD	Min	Max	3d Quartile
Age	57.14	60.00	16.43	14	75	70.00
KV	120.00	120.00	.000	120	120	120.00
mAs	186.71	183.00	77.31	80	299	250.25
Slice No	193.95	190.00	69.51	103	364	245.75
CTDIvol	11.23	12.00	4.098	4	21	14.25
DLP	647.95	526.50	348.09	150	1514	877.00
Turn	12.14	12.00	4.409	6	23	15.25
ED	9.07	7.36	4.87	2.095	21.20	12.28

Table (4.2): shows statistical parameters for CT Chest with contrast

	Mean	Median	STD	Min	Max	3d Quartile
Age	58.42	70.00	18.55	19	75	71.00
KV	120.00	120.00	.000	120	120	120.00
mAs	144.62	136.50	58.49	80	250	185.00
Slice No	133.31	129.00	24.54	103	190	141.75
CTDIvol	8.69	10.00	3.620	4	14	12.00
DLP	702.54	696.00	344.37	257	1474	1015.75
Turn	8.31	8.00	1.594	6	12	9.00
ED	9.84	9.75	4.82	3.59	20.63	14.23

Table (4.3): shows statistical parameters for HRCT

	Mean	Median	STD	Min	Max	3d Quartile
Age	55.76	60.00	16.511	14	75	70.00
KV	120.00	120.00	.000	120	120	120.00
mAs	231.24	259.00	85.82	80	299	299.00
Slice No	242.72	242.00	24.91	200	302	256.50
CTDIvol	12.48	14.00	3.732	4	15	15.00
DLP	387.92	433.00	121.48	150	538	476.50
Turn	15.20	15.00	1.708	12	19	16.00
ED	5.43	6.06	1.70	2.09	7.53	6.66

Table (4.4): shows statistical parameters for Pulmonary Angiography

	Mean	Median	STD	Min	Max	3d Quartile
Age	57.20	56.00	12.84	35	72	70.00
KV	120.00	120.00	.000	120	120	120.00
mAs	185.47	183.00	46.683	126	250	226.00
Slice No	217.80	190.00	92.77	108	364	303.00
CTDIvol	13.53	13.00	3.20	9	21	16.00
DLP	986.73	1006.00	276.12	611	1514	1120.00
Turn	13.67	12.00	5.85	7	23	19.00
ED	13.81	14.09	3.86	8.55	21.20	15.68

Table (4.5): shows the mean of $CTDI_{vol}$, DLP and ED for Chest examination (Chest with contrast, HRCT and PA)

	CTDIvol	DLP	ED
Chest	8.69	702.54	9.84
CTHR	12.48	387.92	5.43
PA	13.53	986.73	13.81

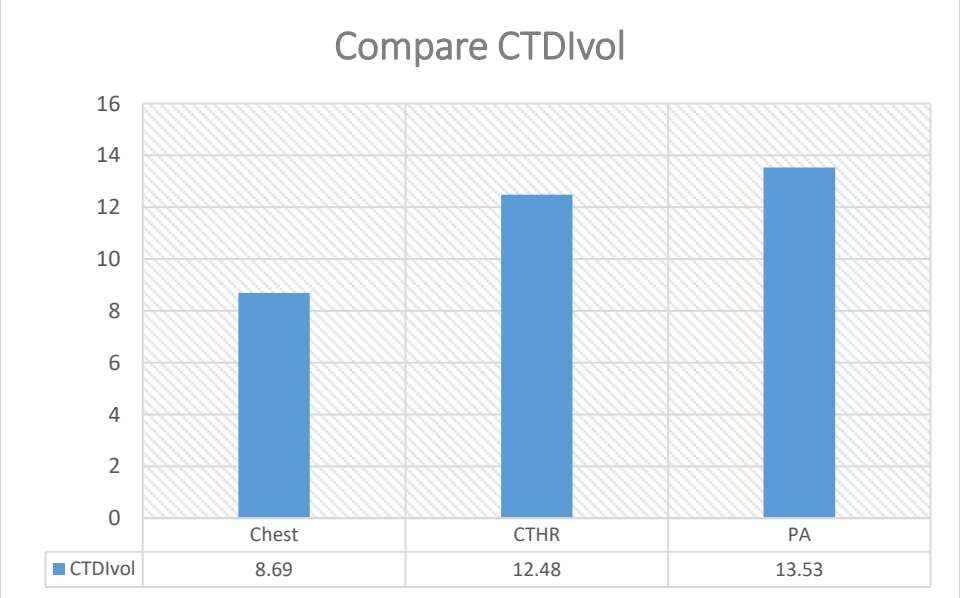

Figure (4.1): shows the comparison between the mean values of $CTDI_{vol}$ in CT Chest examinations

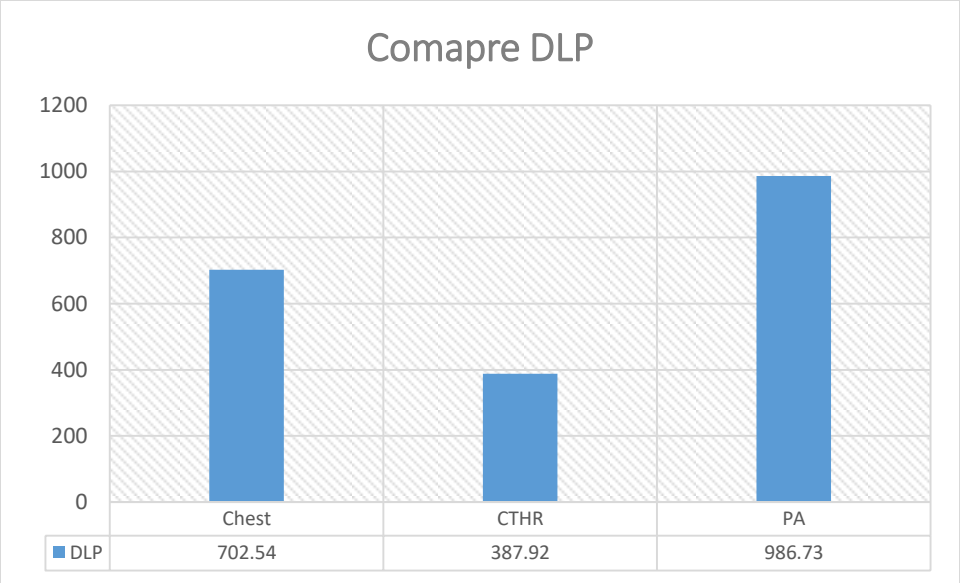

Figure (4.2): shows the comparison between the mean values of DLP in CT Chest examinations

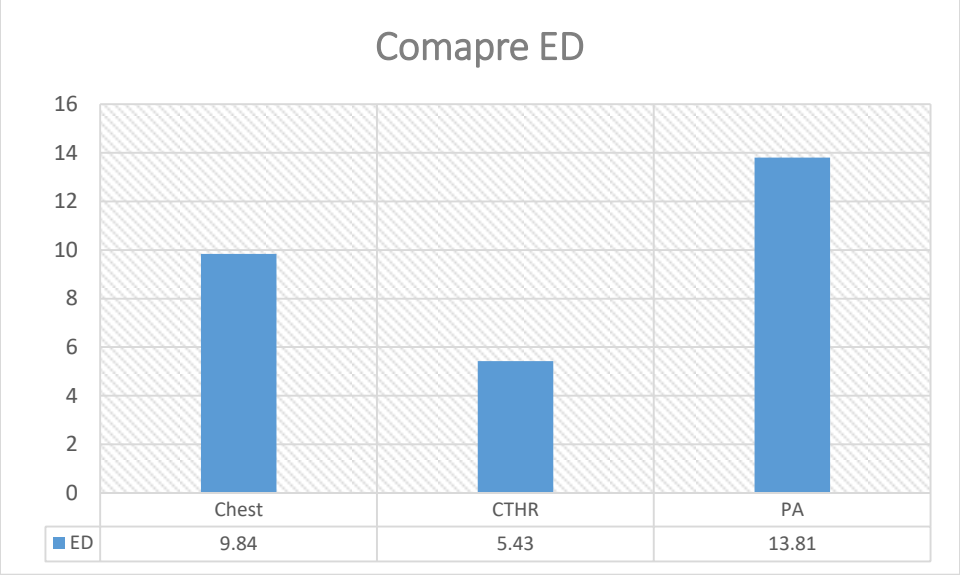

Figure (4.3): shows the comparison between the mean values of ED in CT Chest examinations

Table (4.6): shows compare the $CTDI_{vol,}$ DLP and ED of present study with DRLs from different countries

	CTDIvol	DLP	ED
Present Study 2017	11.23	647.95	9.07
DRLs Japan 2015	15	550	7.7
DRLs Greece 2010	21	430	7.3
DRLs German 2009	20	442	7.2
DRLs UK 2012	14	400	5.8
DRLs Austria 2013	16.2	400	6.7

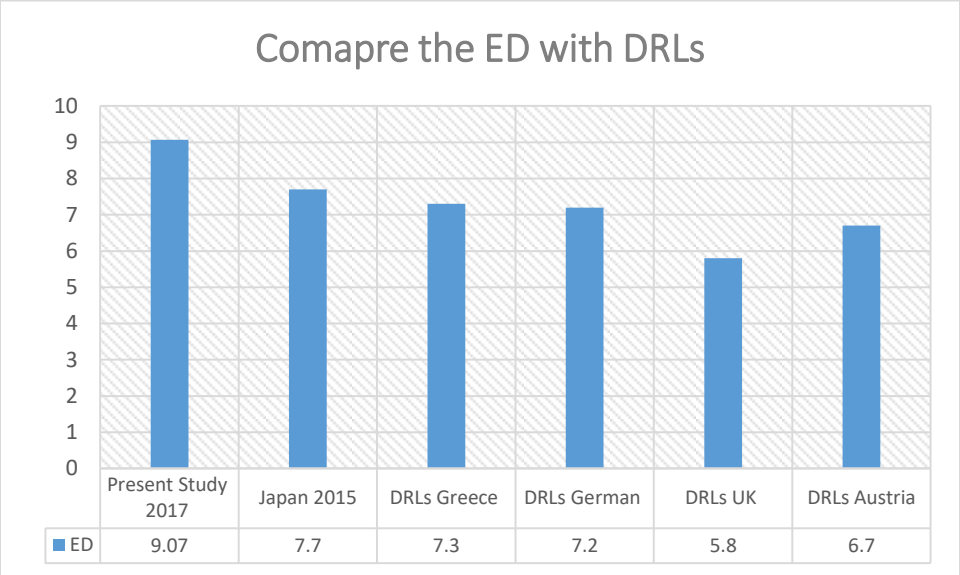

Figure (4.4): shows comparison between values of ED of present study and DRLs from different countries.

Chapter five

Discussion, Conclusion and Recommendations

5.1 Discussion:

This study was involved 66 patients whose underwent CT chest examinations to estimate $CTDI_{vol}$, DLP and ED, and compare the result with DRLs. The results presented in figures and tables as shown above.

The data presented as mean± standard deviation, from table (4.1) the mean of age for all patient in this study was 57.14±16.43 years, Kv 120, mAs 186.71±77.31, number of slices was 193.95±69.51 slice, CTDIvol 11.23±4.098 mGy, DLP 647.95±348.09 mGy/cm and ED 9.07±4.87 mGy.

From table (4.2) the mean patient age in Chest with contrast examination was 58.42±18.55 years, Kv 120, mAs 144.62±58.49 and mean of number of slices was 133.31±24.54 slice, CTDIvol 8.69±3.620 mGy, DLP 702.54±344.37 mGy/cm and ED 9.84±4.82 mGy.

From table (4.3) the mean patient age in HRCT study was 55.76±16.511 years, Kv 120, mAs 231.24±85.82 and mean of number of slices was 242.72±24.91 slice, CTDIvol 12.48±3.732 mGy, DLP 387.92±121.48 mGy/cm and ED 5.43±1.70 mGy.

From table (4.4) the mean patient age in pulmonary angiography procedure was 57.20±12.84 years, Kv 120, mAs 185.47±46.683 and mean of number of slices was 217.80± slice92.77, CTDIvol 13.53±3.20 mGy, DLP 986.73±276.12 mGy/cm and ED 13.81±3.86 mGy.

Table (4.5) represent the values of $CTDI_{vol}$, for Chest with contrast, HRCT and PA and it was 8.69, 12.48 and 13.53 respectively, $CTDI_{vol}$ was higher in

PA than HRCT and Chest with contrast, that's could be because of the exposure factors (Kv and mAs).

DLP and ED values in PA procedure was higher 986.73 and 13.81 than Chest with contrast exam 702.54 and 9.84 and the lowest values was for HRCT procedure 387.92 and 5.43

Variations in these values could be referred for increasing of scan length in PA and Chest with contrast.

Table (4.6) compare of present study with international organization and diagnostic reference level worldwide where the present study (Sudan) found with lower value of $CTDI_{vol}$ comparing with DRLs in different countries, while the DLP and ED was higher than other countries, due to fixation of the exposure factors and increasing of scan length and the all department of radiology in Sudan doesn't activate the AEC options in radiology machines special in Computed Tomography which lead to increasing of patients doses.

5.2 Conclusion:

The purpose of this study was to estimate the patient doses CTDIvol, DLP and Effective dose during CT examinations for chest Modern Medical Center – Khartoum.

The study showed that the calculated dosimetric quantity CTDIvol, DLP and Effective dose was quite high in two examinations comparing with the other one .this discrepancy was mainly due to the scan length used in each exam. Also the study reveals that there is one a specific protocol for CT chest procedures to be followed by all examination. This fact led to the delivery of different doses for patient undergoing the same CT procedure.

The study revealed also that the values of DLP and Effective dose was higher than the DRLs from different countries due to a lack of knowledge about optimization of patient dose and radiation protection aspects.

5.3Recommendations:

A standard protocol for each CT examination should be developed and applied by all hospitals; this will help in minimizing guessing work which in turn would decrease patient dose. All staff should be provided adequate training and retraining both in the field of their specialties as well as in the field of radiation protection.

More studies should be performed for evaluation of the patient dose undergoing CT examinations to cover the other organs which are not considered at this study.

Efforts should be done so as to establish diagnostic reference levels (DRL) for CT examinations in Sudan.

Monitoring of patients doses received during CT examinations should be conducted regularly as part of quality assurance program. Frequent deviations of doses from the set DRLs should be promptly investigated and corrective actions should be identified and implemented.

Avoided repetition test without clinical justification.

Considerate ALARA principle.

References:

BRAUN, F. M., JOHNSON, T. R., SOMMER, W. H., THIERFELDER, K. M. & MEINEL, F. G. 2015. Chest CT using spectral filtration: radiation dose, image quality, and spectrum of clinical utility. *Eur Radiol,* 25**,** 1598-606.

CARRIER, G., FRECHETTE, E., UGALDE, P. & DESLAURIERS, J. 2007. Correlative anatomy for the sternum and ribs, costovertebral angle, chest wall muscles and intercostal spaces, thoracic outlet. *Thorac Surg Clin,* 17**,** 521-8.

CHAE, I. H., KIM, Y., LEE, S. W., PARK, J. E., SHIM, S. S. & LEE, J. H. 2014. Standard chest CT using combined automated tube potential selection and iterative reconstruction: image quality and radiation dose reduction. *Clin Imaging,* 38**,** 641-7.

CLEMENS, M. W., EVANS, K. K., MARDINI, S. & ARNOLD, P. G. 2011. Introduction to chest wall reconstruction: anatomy and physiology of the chest and indications for chest wall reconstruction. *Semin Plast Surg,* 25**,** 5-15.

DE MARGERIE-MELLON, C., DE BAZELAIRE, C., MONTLAHUC, C., LAMBERT, J., MARTINEAU, A., COULON, P., DE KERVILER, E. & BEIGELMAN, C. 2016. Reducing Radiation Dose at Chest CT: Comparison Among Model-based Type Iterative Reconstruction, Hybrid Iterative Reconstruction, and Filtered Back Projection. *Acad Radiol,* 23**,** 1246-54.

ELLIS, H. 2007. The applied anatomy of chest drain insertion. *Br J Hosp Med (Lond),* 68**,** M44-5.

GABUSI, M., RICCARDI, L., ALIBERTI, C., VIO, S. & PAIUSCO, M. 2016. Radiation dose in chest CT: Assessment of size-specific dose estimates based on water-equivalent correction. *Phys Med,* 32**,** 393-7.

KALENDER, W. A. 2000. Computed tomography: fundamentals, system technology, image quality, applications. *Computed Tomography: Fundamentals, System Technology, Image Quality, Applications, by Willi A. Kalender, pp. 220. ISBN 3-89578-081-2. Wiley-VCH, November 2000.***,** 220.

KARARGYRIS, A., ANTANI, S. & THOMA, G. 2011. Segmenting anatomy in chest x-rays for tuberculosis screening. *Conf Proc IEEE Eng Med Biol Soc,* 2011**,** 7779-82.

LARKE, F. J., KRUGER, R. L., CAGNON, C. H., FLYNN, M. J., MCNITT-GRAY, M. M., WU, X., JUDY, P. F. & CODY, D. D. 2011. Estimated radiation dose associated with low-dose chest CT of average-size participants in the National Lung Screening Trial. *American Journal of Roentgenology,* 197**,** 1165-1169.

LAURI, H. 2017. High-resolution CT of the lungs: Indications and diagnosis. *Duodecim,* 133**,** 549-56.

LI, X., SAMEI, E., SEGARS, W. P., STURGEON, G. M., COLSHER, J. G. & FRUSH, D. P. 2011. Patient-specific radiation dose and cancer risk for pediatric chest CT. *Radiology,* 259**,** 862-74.

LIM, H. K., HA, H. I., HWANG, H. J. & LEE, K. 2016. Feasibility of high-pitch dual-source low-dose chest CT: Reduction of radiation and cardiac artifacts. *Diagn Interv Imaging,* 97**,** 443-9.

LIVINGSTONE, R. S., PRADIP, J., DINAKRAN, P. M. & SRIKANTH, B. 2010. Radiation doses during chest examinations using dose modulation techniques in multislice CT scanner. *Indian J Radiol Imaging,* 20**,** 154-7.

MACIA-SUAREZ, D., SANCHEZ-RODRIGUEZ, E., LOPEZ-CALVINO, B., DIEGO, C. & POMBAR, M. 2017. Low-voltage chest CT: another way to reduce the radiation dose in asbestos-exposed patients. *Clin Radiol,* 72**,** 797 e1-797 e10.

MAYO, J. R., HARTMAN, T. E., LEE, K. S., PRIMACK, S. L., VEDAL, S. & MULLER, N. L. 1995. CT of the chest: minimal tube current required for good image quality with the least radiation dose. *AJR Am J Roentgenol,* 164**,** 603-7.

MAYO, J. R., JACKSON, S. A. & MULLER, N. L. 1993. High-resolution CT of the chest: radiation dose. *AJR Am J Roentgenol,* 160**,** 479-81.

MAYO, J. R., KIM, K. I., MACDONALD, S. L., JOHKOH, T., KAVANAGH, P., COXSON, H. O. & VEDAL, S. 2004. Reduced radiation dose helical chest CT: effect on reader evaluation of structures and lung findings. *Radiology,* 232**,** 749-56.

METTLER JR, F. A., WIEST, P. W., LOCKEN, J. A. & KELSEY, C. A. 2000. CT scanning: patterns of use and dose. *Journal of radiological Protection,* 20**,** 353.

PARKER, M. S., KELLEHER, N. M., HOOTS, J. A., CHUNG, J. K., FATOUROS, P. P. & BENEDICT, S. H. 2008. Absorbed radiation dose of the female breast during

diagnostic multidetector chest CT and dose reduction with a tungsten-antimony composite breast shield: preliminary results. *Clin Radiol,* 63**,** 278-88.

PROTECTION, R. 1999. 109: Guidance on diagnostic reference levels (DRLs) for Medical Exposures. *Luxembourg: European Communities*.

RAMJATTAN, N. A. & MAKARYUS, A. N. 2017. Coronary CT Angiography. *StatPearls.* Treasure Island (FL).

RIQUET, M., MORDANT, P., PRICOPI, C., ACHOUR, K. & LE PIMPEC BARTHES, F. 2013. [Anatomy, micro-anatomy and physiology of the lymphatics of the lungs and chest wall]. *Rev Pneumol Clin,* 69**,** 102-10.

ROMANS, L. E. 2010. *Computed tomography for technologists: Exam review*, Lippincott Williams & Wilkins.

SEERAM, E. 2015. *Computed Tomography-E-Book: Physical Principles, Clinical Applications, and Quality Control*, Elsevier Health Sciences.

SINGH, S., DIGUMARTHY, S. R., BACK, A., SHEPARD, J. A. & KALRA, M. K. 2013. Radiation dose reduction for chest CT with non-linear adaptive filters. *Acta Radiol,* 54**,** 169-74.

SINGH, S., KALRA, M. K., THRALL, J. H. & MAHESH, M. 2011. Pointers for optimizing radiation dose in chest CT protocols. *J Am Coll Radiol,* 8**,** 663-5.

STAMM, G. & NAGEL, H. D. 2002. CT-expo--a novel program for dose evaluation in CT. *RoFo: Fortschritte auf dem Gebiete der Rontgenstrahlen und der Nuklearmedizin,* 174**,** 1570-1576.

SUSSMANN, A. R. & KO, J. P. 2010. Understanding chest radiographic anatomy with MDCT reformations. *Clin Radiol,* 65**,** 155-66.

ZANCA, F., DEMETER, M., OYEN, R. & BOSMANS, H. 2012. Excess radiation and organ dose in chest and abdominal CT due to CT acquisition beyond expected anatomical boundaries. *Eur Radiol,* 22**,** 779-88.

ZHI, A. H., DAI, R. P., MA, W. G., ZHANG, P., LV, B. & JIANG, S. L. 2017. CT angiography for diagnosis and subcategorization of unroofed coronary sinus syndrome. *J Thorac Dis,* 9**,** 3946-3955.

ZHU, X., YU, J. & HUANG, Z. 2004. Low-dose chest CT: optimizing radiation protection for patients. *AJR Am J Roentgenol,* 183**,** 809-16.

Appendix:

sex	Age	KV	mAs	collimation	slice number	slice thickness	scan length	CTDIvol	DLP	turn	Pitch

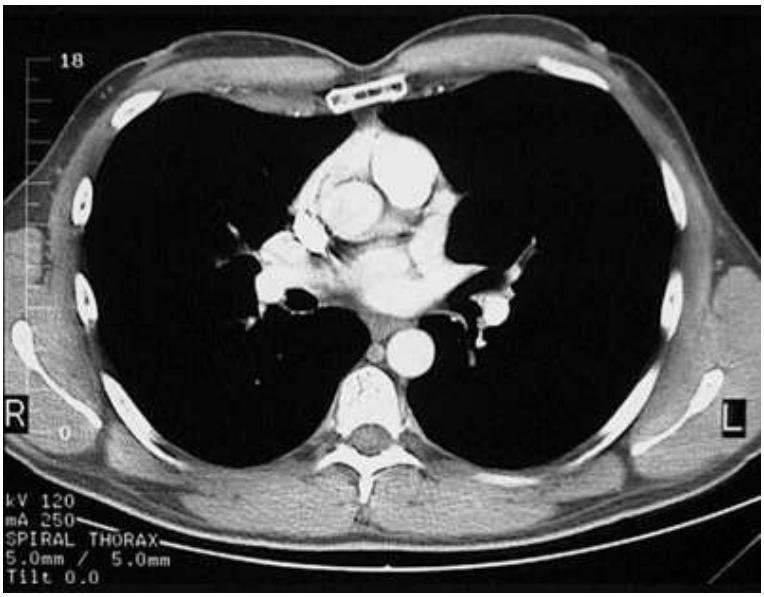

Picture.1: shows Chest with contrast exam slice for 40 years old male patient

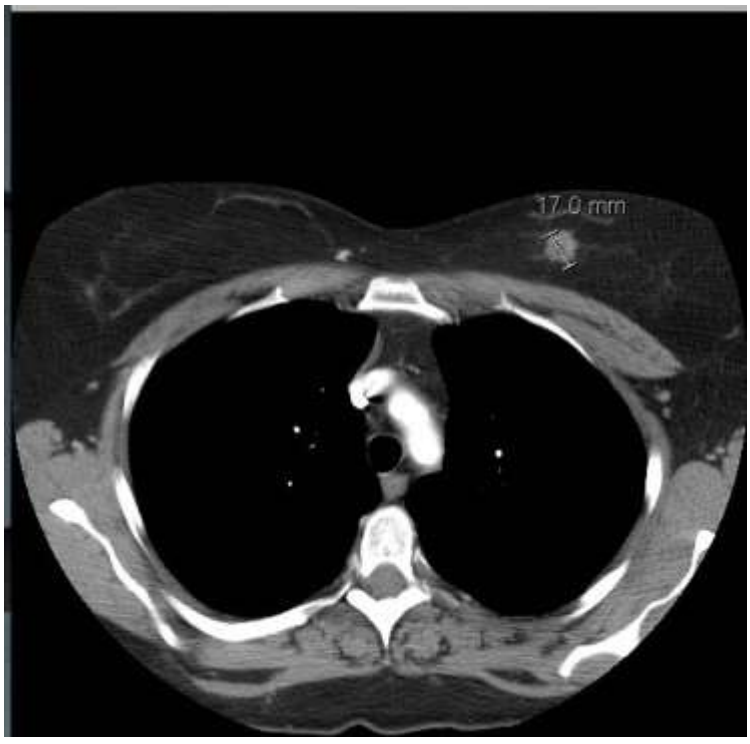

Picture.2: shows Chest with contrast exam slice for 38 years old female patient

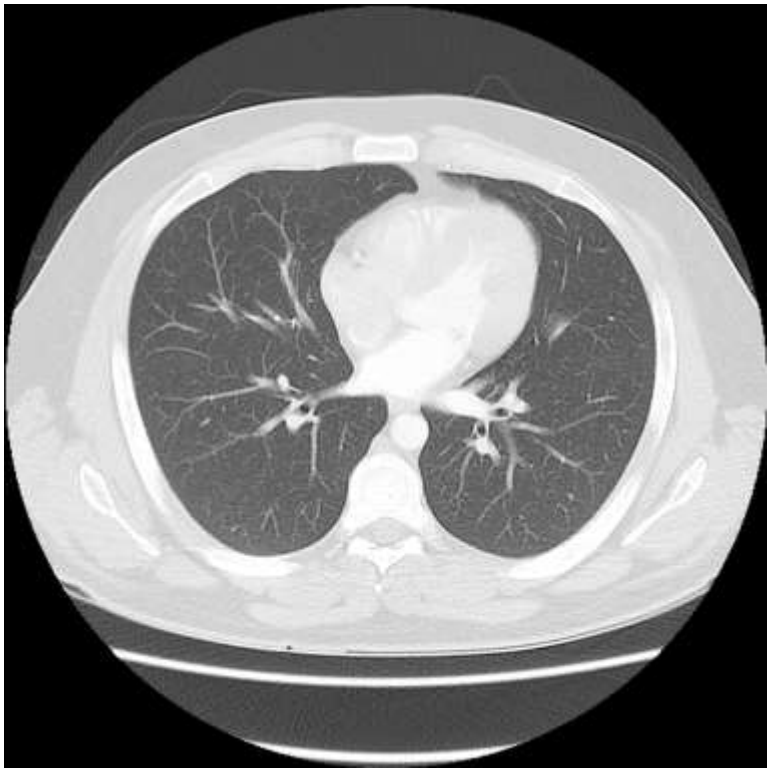

Picture.3: shows HRCT exam slice for 36 years old male patient

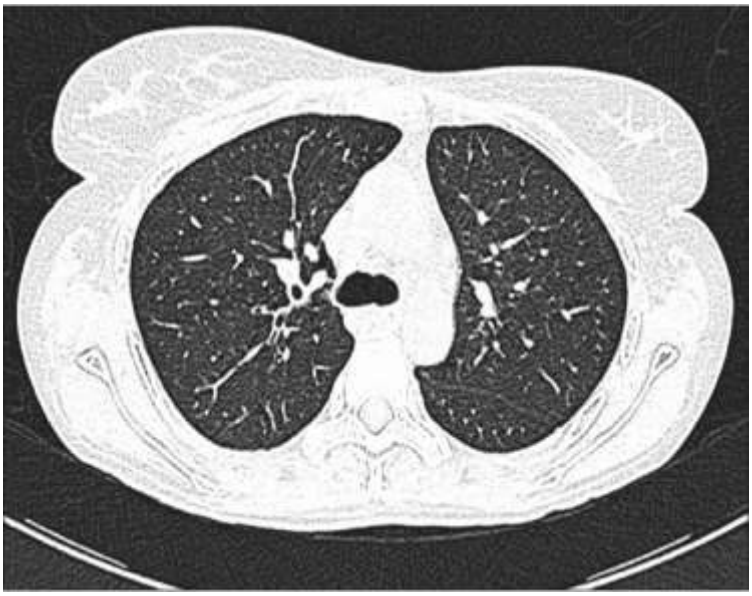

Picture.4: shows HRCT exam slice for 76 years old female patient

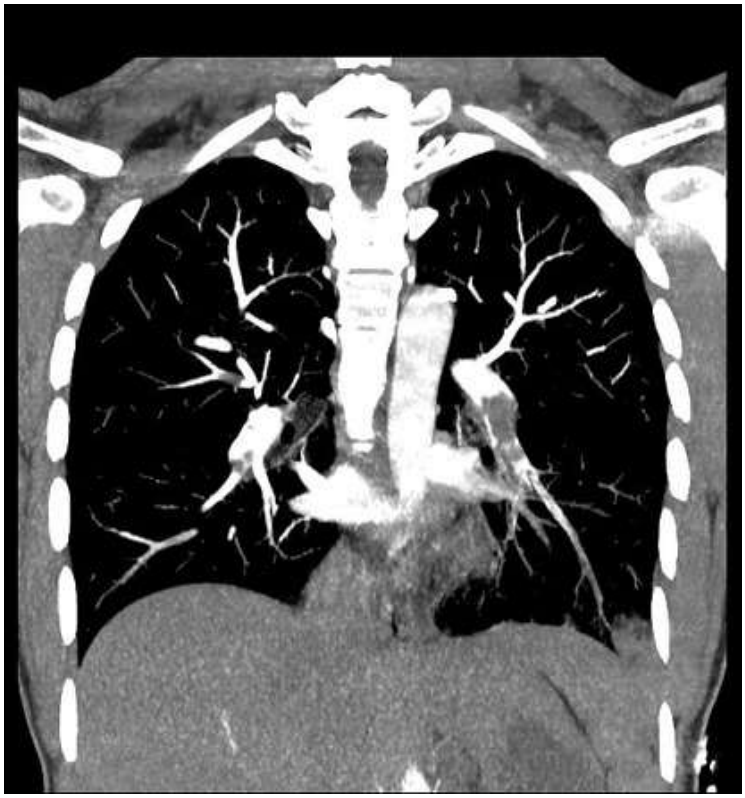

Picture.5: shows PA exam for 52 years old male patient

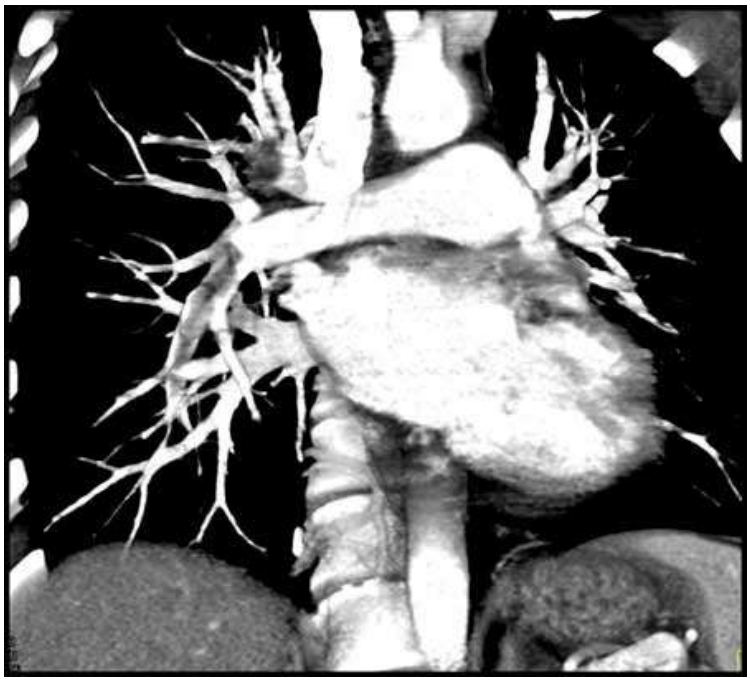

Picture.6: shows PA exam for 48 years old female patient